Design of a SENSE-Optimized High-Sensitivity MRI Receive Coil for Brain Imaging

Jacco A. de Zwart,[1] Patrick J. Ledden,[2] Peter Kellman,[3] Peter van Gelderen,[1] and Jeff H. Duyn[1*]

An 8-channel receive-only detector array was developed for SENSE MRI of human brain. The coil geometry was based on a gapped element design and used ultra-high impedance preamplifiers for mutual decoupling of the elements. Computer simulations of the electric and magnetic fields showed that excellent signal-to-noise ratio (SNR) and SENSE performance could be achieved by placing the coil elements close to the head and maintaining a substantial gap between the elements. Measurements with a 1.5 T prototype coil showed a 2.7-fold improvement of the SNR averaged over the brain compared to a conventional quadrature birdcage receive coil and an average geometrical noise amplification factor (*g*-value) of 1.06 and 1.38 for rate-2 and rate-3 SENSE, respectively. Magn Reson Med 47: 1218–1227, 2002. Published 2002 Wiley-Liss, Inc.†

Key words: MRI; parallel imaging; SENSE; brain imaging; RF coil; sensitivity; SNR

The receive coil is one of the most important elements of MRI hardware, as it determines the ultimately achievable image signal-to-noise ratio (SNR). Various types of MRI receive coils exist, including the birdcage design (1) and the phased array design (2). For MRI of the human brain the birdcage coil is most commonly used, since it is easy to handle, provides a uniform $\mathbf{B}_1$ field, has robust operation, and can be used in both transmit and receive mode.

The recent surge in the application of parallel imaging techniques based on simultaneous reception through multiple receive channels has invited a redesign of the MRI signal detector. The effectiveness of parallel imaging techniques such as SENSE (3) and SMASH (4) is dependent on proper design of the receive coils, which ultimately determine the image artifact level and SNR.

Receive coils for parallel imaging techniques consist of a number of elements or channels, each working more or less independently and sensitized to a different segment of the field of view (FOV). The coils generally work in combination with a separate, larger transmit coil with uniform excitation profile over the entire FOV. An important advantage of multi-channel receive coils for brain imaging is the fact that they provide high SNR in the peripheral cortex and that, when combined with parallel imaging, they facilitate the use of single-shot MRI techniques such as EPI (5) for applications like diffusion imaging (6) and BOLD functional imaging (7).

A limited number of multi-channel coils have been designed specifically for human brain imaging, either focusing on optimizing SNR in specific regions or the entire brain (8–11). The design of a SENSE-optimized 6-channel receive coil for cardiac imaging has been described recently (12). However, until now no comprehensive optimization of multichannel coils for parallel imaging in the brain has been reported in the literature. Discussed in the following is how SNR and SENSE requirements are dealt with in the design of an 8-channel brain receive array.

MATERIALS AND METHODS

Design Criteria

The two main criteria in the design of the receive-only brain coil were to obtain maximal SNR and FOV reduction. In addition, the coil was to provide whole-brain coverage and perform well both at various SENSE acceleration rates and in conventional imaging, thus avoiding the need to switch between coils in studies that only partly employ SENSE.

The attainable FOV reduction factor in SENSE, also called the acceleration rate, is governed by the so-called noise amplification factor, *g* (3,12), which indicates the SNR penalty incurred by SENSE reconstruction (excluding the data reduction aspect). Factor *g* is spatially varying and depends strongly on the number of coil elements, as well as the size, shape, and positioning of the elements. In general, lower *g*-values are obtained when the $\mathbf{B}_1$ profiles of the individual elements are more orthogonal (the different coil elements are sensitive to different areas of the brain). In practice, reduction of *g* (to allow an increase of SNR and acceleration rate) can be achieved by increasing the number of coil elements, avoiding element overlap, and minimizing coupling between elements.

An important constraint in the design of MR receive arrays is the number of available receive channels. In most clinical scanners today the maximum number of receive channels is 4 to 8. Therefore, in most of the simulations, as well as the final construction and evaluation, 8 available channels were assumed.

Design Approach

An important issue that needed to be addressed in the design of the multi-channel brain coil was inductive coupling between coil elements (2), which can compromise performance. Previous multi-element coil designs (2,8–10) achieved decoupling by using a "magic overlap" (2) of

[1]Advanced MRI, Laboratory of Functional and Molecular Imaging, NINDS, National Institutes of Health, Bethesda, Maryland.

[2]Nova Medical, Wakefield, Massachusetts.

[3]Laboratory of Cardiac Energetics, NHLBI, National Institutes of Health, Bethesda, Maryland.

*Correspondence to: Jeff Duyn, Advanced MRI/LFMI/NINDS, National Institutes of Health, Bldg. 10, Rm. B1D-118 - MSC 1065, 10 Center Drive, Bethesda, MD 20892-1065. E-mail: jhd@helix.nih.gov

Received 15 October 2001; revised 4 January 2002; accepted 31 January 2002.

DOI 10.1002/mrm.10169

Published online in Wiley InterScience (www.interscience.wiley.com).

neighboring coil elements, combined with the use of high-impedance preamplifiers (2). Although this approach works well under certain conditions, it poses restrictions on the coil design. In the following, negligible coupling between adjacent coil elements was achieved without the need for "magic overlap" by using ultra-high impedance preamplifiers (13). This provides great flexibility in positioning of the coils and ultimately allows for lower g values and higher SNR.

Another factor in the design approach was that splitting of elements in the B_0-direction was avoided, since this leads to undesirable signal dropouts between the elements. Therefore, the design of the coil was constrained to a single row of elements wrapped around the head, with constant inter-element gap. Lastly, similar-sized elements were used to simplify construction and to obtain a more uniform combined $\mathbf{B}_1$ profile.

Simulations

To investigate SNR characteristics and SENSE performance of a multi-element receive coil for brain imaging as a function of coil geometry, magnetic and electric field simulations were performed in IDL (Research Systems International, Boulder, CO). The human head was modeled as a cylindrical object with uniform conductivity σ. The coil consisted of a variable number of rectangular loops of identical shape, positioned on a cylinder, with a constant interelement spacing (see Fig. 1). From the magnetic vector potential $\mathbf{A}$, both magnetic field profiles $\mathbf{B}$, and standard deviation of the sample noise amplitude N_s (14) were derived using:

$$N_S \propto \sqrt{R_S} \propto \sqrt{\sigma \cdot \omega^2 \int_V \mathbf{A} \cdot \mathbf{A} d\mathbf{r}} \qquad [1a]$$

$$\mathbf{B} = \vec{\nabla} \times \mathbf{A} \qquad [1b]$$

with R_s the equivalent noise resistance and ω the NMR resonance frequency. In Eq. [1a], magnetic and electrostatic noise sources are neglected and the integral is performed over the entire object volume V.

The SNR of a single coil element i is proportional to the ratio of its signal amplitude (S_i) and its total noise amplitude standard deviation (N_i):

$$\mathrm{SNR}_i = \frac{|S_i|}{N_i} \propto \frac{\omega^2 |\mathbf{B}_{1,i}|}{\sqrt{N_{s,i}^2 + N_{c,i}^2 + N_{r,i}^2}} \qquad [2]$$

with $N_{s,i}$, $N_{c,i}$, and $N_{r,i}$ representing sample, coil, and receiver (including preamplifier and matching circuitry) noise standard deviation associated with channel i, respectively. $\mathbf{B}_{1,i}$ is the x,y-component of the magnetic field vector $\mathbf{B}$. In the following, we assume that receiver noise can be made sufficiently small and neglected. Under conditions that sample noise is much large than coil noise, a combination of Eqs. [1] and [2] leads to:

$$\mathrm{SNR}_i \propto \frac{\omega |\mathbf{B}_{1,i}|}{\sqrt{\sigma \int_V A_i \cdot A_i dr}}. \qquad [3]$$

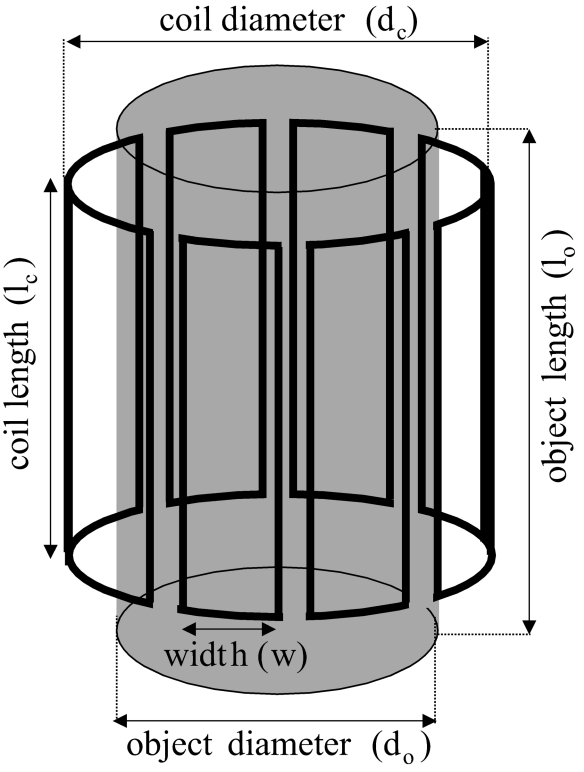

FIG. 1. Schematic layout of conductors forming eight coil elements, used for the simulations. Rectangular coil elements with axial length l_c and width w were laid out on a cylinder with diameter d_c and spaced with a constant interelement gap. A cylindrical object with uniform conductivity σ, diameter d_o and length l_o was placed coaxially within the coil cylinder.

Coil performance was determined from the SNR of the root-sum-of squares (RSS) combined (2) signals of the individual coil elements (SNR_c) and g (3):

$$\mathrm{SNR}_c = \sqrt{\mathbf{S}^H \boldsymbol{\Psi}^{-1} \mathbf{S}} \qquad [4]$$

$$g_\rho = \sqrt{[(\boldsymbol{\Sigma}^H \boldsymbol{\Psi}^{-1} \boldsymbol{\Sigma})^{-1}]_{\rho,\rho} (\boldsymbol{\Sigma}^H \boldsymbol{\Psi}^{-1} \boldsymbol{\Sigma})_{\rho,\rho}} \qquad [5]$$

with $\mathbf{S}$ a vector containing the signals S_i from the individual coil elements, $\boldsymbol{\Sigma}$ the coil sensitivity matrix (3), constituting a reformatted version of $\mathbf{S}$, with number of rows and columns determined by the number of coil elements and acceleration rate, respectively, and $\boldsymbol{\Psi}$ the noise correlation matrix. The parameter g_ρ contains the g values for the ρ^{th} region in the unaliased image (e.g., for rate 3 SENSE ρ takes on values 0, 1, and 2 and g_ρ is defined over an image section covering $\frac{1}{3}$ of the FOV). Assuming only electric (no inductive) coupling between elements, $\boldsymbol{\Psi}$ can be calculated from:

$$\Psi_{ij} = \sigma \cdot \omega^2 \int_V \mathbf{A}_i \cdot \mathbf{A}_j d\mathbf{r}. \qquad [6]$$

The calculations were performed over a 3D grid consisting of 60 × 60 × 60 elements covering the volume of

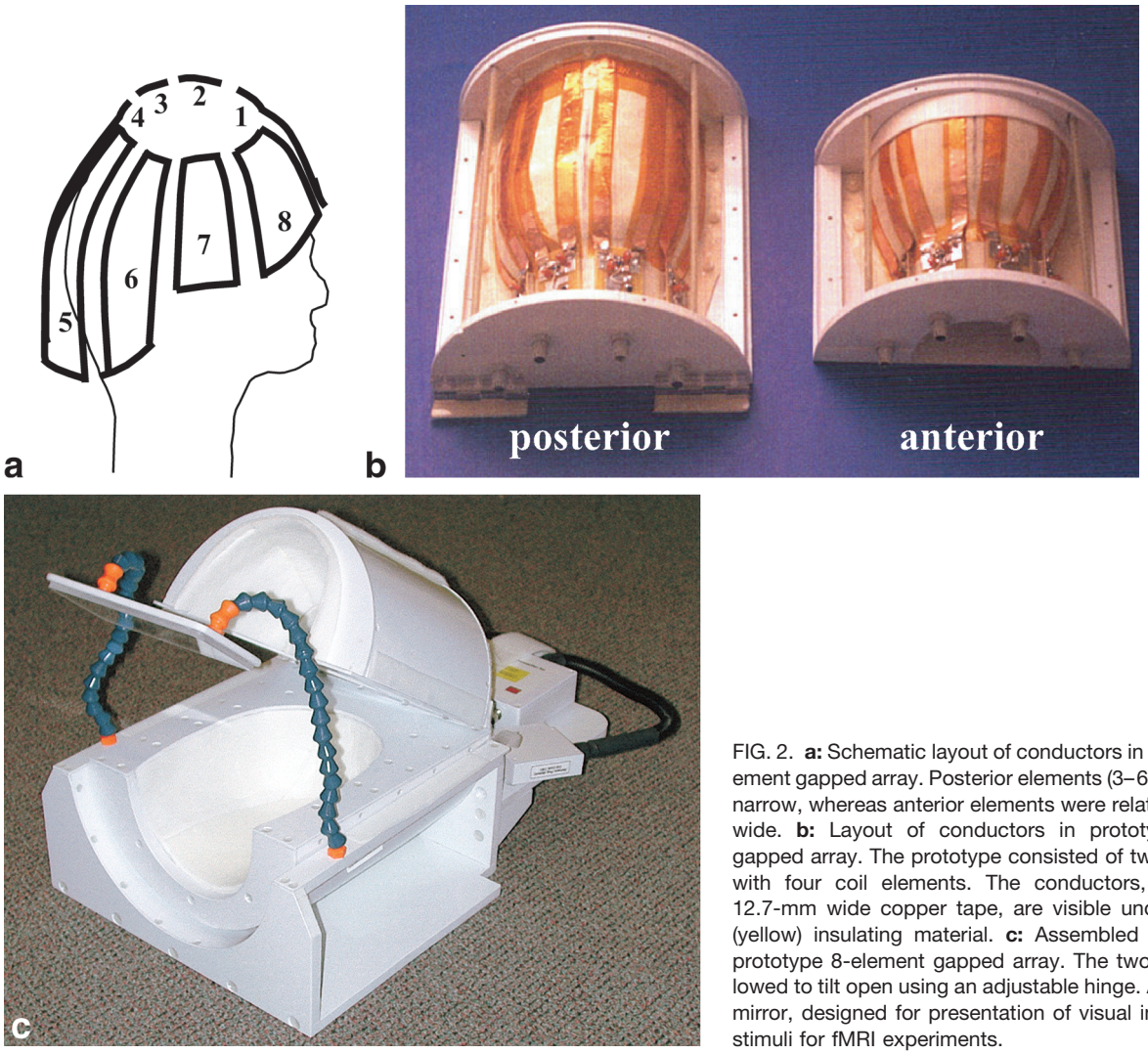

FIG. 2. **a:** Schematic layout of conductors in prototype 8-element gapped array. Posterior elements (3–6) were long and narrow, whereas anterior elements were relatively short and wide. **b:** Layout of conductors in prototype 8-element gapped array. The prototype consisted of two halves, each with four coil elements. The conductors, made out of 12.7-mm wide copper tape, are visible under the kapton (yellow) insulating material. **c:** Assembled version of the prototype 8-element gapped array. The two halves are allowed to tilt open using an adjustable hinge. Also visible is a mirror, designed for presentation of visual information and stimuli for fMRI experiments.

interest, unless otherwise stated. At this grid size, adequate accuracy for the intended optimization of coil parameters was obtained. Larger grid sizes did not significantly alter results, but rather resulted in often prohibitive computational times and memory usage. The default simulation parameters were (see Fig. 1 for an explanation of symbols): $d_o = 0.85$; $l_o = 0.85$; $d_c = 1.1d_o$; $l_c = 0.7d_c$; number of coil elements (n) = 8; interelement gap

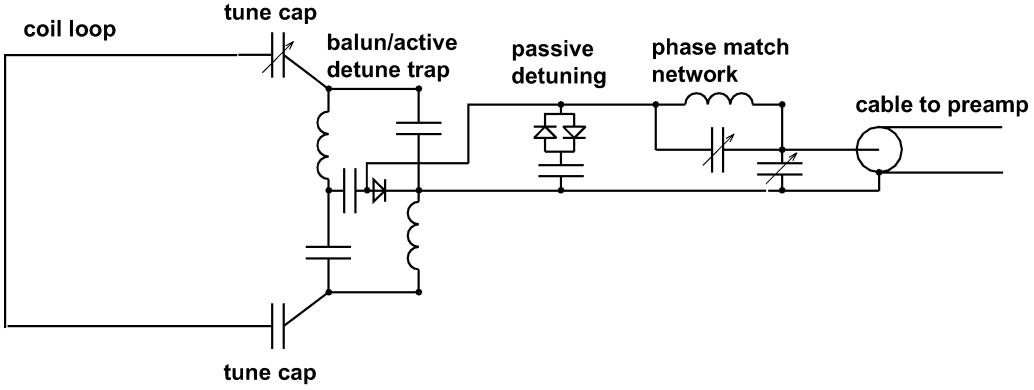

FIG. 3. Coil tuning and matching network, connecting each coil element to a preamplifier. Phase match network and cable are part of an effective $\frac{1}{4}\lambda$, 50Ω transmission line, translating high impedance at the preamplifier into low impedance. A balun transforms the low impedance (looking into the phase match network) into high impedance at the coil terminals. Active and passive detuning prevent currents from running in the coil loop and towards preamplifier during transmission.

("gap") = 0.5. SNR and *g*-factors were calculated over a volume covering the central 60% of the object in axial direction. The parameters that were varied were *n*, "gap," and d_c. With increases in "gap," the coil width was reduced to maintain overall array diameter. Values of "gap" were expressed as a fraction of the element width. With variation of coil diameter d_c, the coil length l_c was varied proportionally and a $90 \times 90 \times 90$ matrix size was used. The latter was done to maintain resolution at the larger FOVs required for this simulation. In all simulations it was assumed that coupling between elements was negligible, independent of the actual level of mutual inductance.

Coil Construction

To investigate the conditions under which sample noise is the dominant noise source, a series of 10 square coils was built, ranging in diameter from 2.54 cm (1.0 inch) to 12.70 cm (5.0 inch). After tuning to 63.6 MHz, the width of the coil resonance was measured for both unloaded and loaded (coil at approximately 3 mm from the human head) conditions using an HP 4195A network analyzer (Hewlett-Packard, Palo Alto, CA). From these data, sample and coil noise resistance were calculated.

To evaluate the practical feasibility of the gapped element design and determine SNR values and *g* attainable in human brain imaging, an 8-element receive-only brain coil was constructed for operation at 63.6 MHz (1.5 T) (Fig. 2a–c). Since the simulation indicated improved SNR and *g* with a tight-fitting (small diameter) coil, an anatomically shaped, 2-mm thick former was constructed which closely fitted the average head size (largest anterior–posterior dimension 22 cm, largest left–right dimension 18 cm). The former was divided into two segments (a posterior and an anterior segment) to allow adjustment to varying head sizes. On each of the segments four coil loops were laid out on the outside of the fiberglass former using 12.7 mm wide, 50 μm thick copper tape. In order to minimize sample noise without sacrificing brain coverage, following the shape of the brain (in axial direction) was attempted while laying out the elements. This resulted in the axial length of the anterior elements being smaller than that of the posterior elements (Fig. 2a,b). To partially compensate for the shorter axial length the anterior elements were made slightly wider than the corresponding posterior elements. The elements were spaced with an inter-element gap equaling roughly 50% of the element width (measured on conductor center) in the axial plane. The coils all had very similar surface areas (75 ± 10 cm^2) and inductances (250 ± 25 nH). Each coil was matched to 50Ω with a combined active detuning trap, lumped element balun circuit (Fig. 3). Passive crossed diodes offered additional protection in the event of failure of the primary active PIN diode circuit. To minimize inductive coupling (C_m), the coils were connected to custom-made ultrahigh-impedance (>3 kΩ real), low noise (noise figure = 0.5 dB) preamplifiers (model NMP-1, Nova Medical, Wakefield, MA), through a 15-cm long section of RG-58 remove coaxial cable and phase-matching circuitry. This resulted in an effective $\frac{1}{4}\lambda$, 50Ω transmission line translating the 3 kΩ input impedance of the preamplifier into a minimum value (below 1Ω, see below) across the detuning PIN diode. Additional triaxial common mode cable traps were placed after the preamplifiers. Preamplifier decoupling resulted in a 35.45 dB drop in coupling (results not shown). Ratios of unloaded coil quality factor, *Q*, vs. human-head-loaded *Q* were around 5, validating the assumption in Eq. [3] that contribution of noise originating from sources other than the sample can be made small under practical conditions.

The inductive coupling, C_m, was estimated from (2):

$$C_m = \frac{j\omega L k_m}{R_1 + X^2/R_p} \qquad [7]$$

with *L* the coil inductance, k_m the magnetic coupling coefficient (mutual inductance), R_1 the coil impedance, R_p the input impedance of the preamplifier as viewed from its connection to the matching network, and *X* the impedance of the matching network components. Matching to 50Ω cable ($X^2 = 50\ R_1$) leads to:

$$C_m = \frac{j\omega L k_m}{R_1(1 + R'_p/50)} \approx \frac{50 Q k_m}{R'_p} \qquad [8]$$

where R'_p is the input impedance at the preamplifier, which transforms to R_p according to $R_p \times R'_p = 50^2$ due to the use of 50Ω cable of $\frac{1}{4}\lambda$ length to connect preamplifier and matching network.

Assuming $R'_p = 3$ kΩ and $Q = 70$ (close to values measured on human head), we find: $C_m = 1.2k_m$. Since the magnetic coupling coefficient k_m is generally only a small fraction of 1 for nonoverlapping adjacent coils, e.g., below 0.02 for square elements with "gap" = 0.5 (estimated from fig. 9 in Ref. 2), this suggests that low inductive coupling can be practically achieved using preamplifier decoupling, even in neighboring elements of a gapped array.

MR Measurements

MRI scans were performed on a 1.5 T Siemens Sonata scanner (Siemens Medical Systems, Erlangen, Germany) operating on the Numaris 4 platform. The scanner had eight receiver channels, each with 1 MHz bandwidth. Human imaging was performed on a normal, healthy volunteer. This study was approved by the Institutional Review Board of the National Heart, Lung and Blood Institute. Gradient echo imaging was performed with 256×256 matrix size, 24×24 cm FOV, 4 mm slice thickness, 20 ms TE, 500 ms TR, flip-angle 30°, 133 kHz bandwidth. SNR measurements were performed on human brain using the prototype 8-channel brain coil and also using the standard Siemens head coil (CP head array, model #1P3146037). To compare performance with the standard birdcage coil from a different vendor, SNR measurements with identical scan parameters, and on the same subject, were also performed with a standard General Electric quadrature birdcage head coil (model #46-28211186202) using a 1.5 T GE echospeed system (GE Medical, Milwaukee, WI) running on the LX 8.4 platform at 63.8 MHz. For calculation of noise levels and noise correlation between

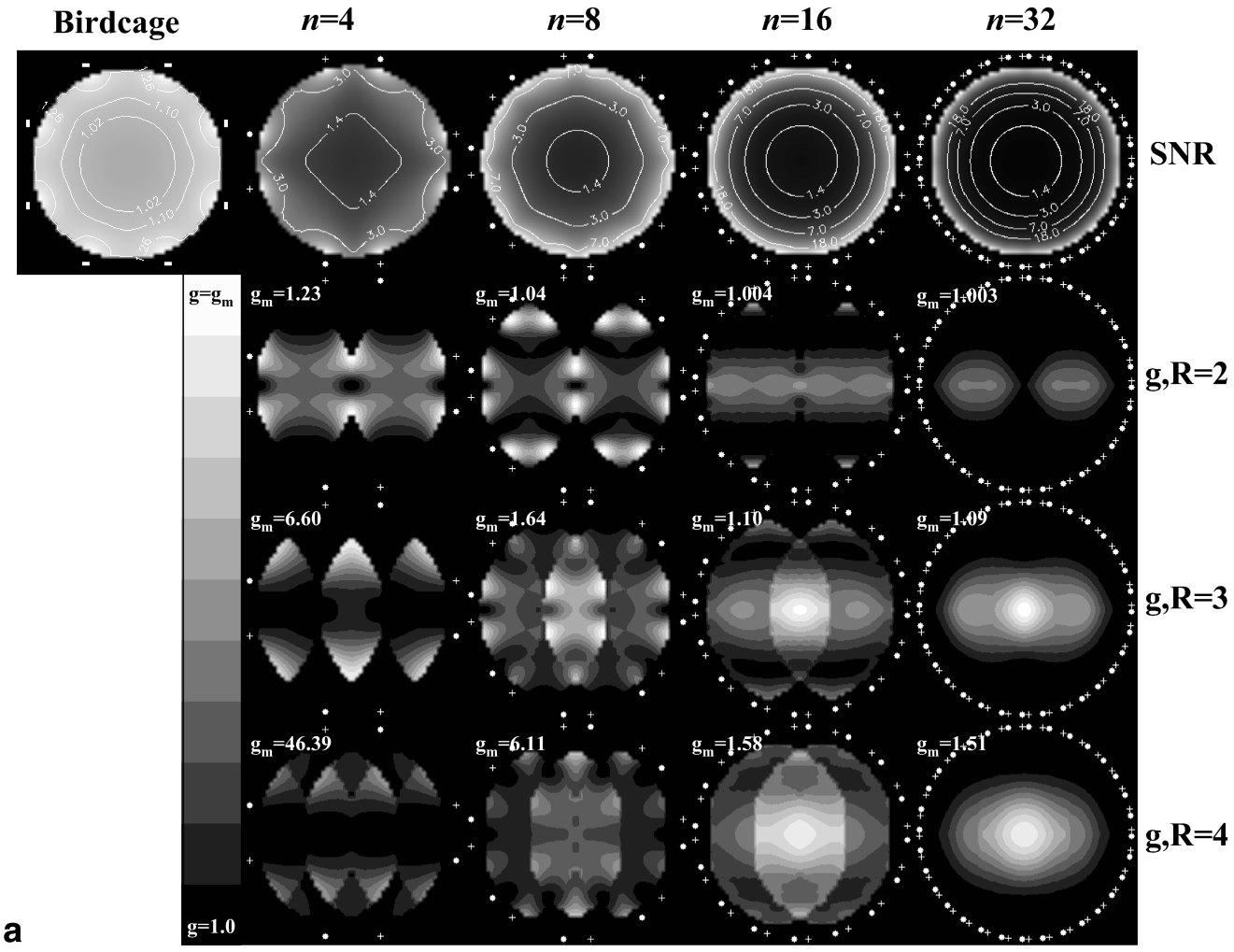

FIG. 4. Simulation of SNR and *g* in brain coil under various conditions (see text). SENSE direction was left to right. Varied were number of coil elements *n* (**a**), interelement gap (**b**), and coil diameter (**c**). Other parameters were kept constant. Displayed are SNR and *g* in an axial slice through the center of the object. Conductor positions are marked with plus signs and filled circles, surrounding the object. In the SNR maps (top rows), levels are relative to the SNR in the center of an 8-rung birdcage coil with $d_c = 1.1d_o$, $l_c = 0.7d_c$ and indicated with annotated iso-intensity contours. In **a**, SNR was scaled to the maximum values for each configuration and the display scale of *g* was adjusted per image, with upper level g_{max} indicated at the top of each image and lower level fixed at 1.00. The simulated SNR of an 8-element element birdcage coil is shown in the top-left corner as reference. In **b** and **c**, scaling was kept constant over geometries (within rows) and indicated at the right of each row. Note that in **c** some of the conductor elements are not visible due to the limited FOV of the image.

channels, noise data was acquired by selecting a slice outside the head.

MRI Data Analysis

Combination of the individual coil images from the 8-channel coil was performed by RSS combining following Eq. [4], with **S** derived directly from the complex coil images. In this equation, the noise covariance matrix, $\mathbf{\Psi}$, was estimated from the noise data using:

$$\hat{\Psi}_{ij} = \frac{\sum_{m=1}^{N} r_i(m) r_j^*(m)}{N} \qquad [9]$$

with r_i(m) the complex signal value from coil *i* in data point *m*. Equation [9] was also applied to calculate noise power levels for the birdcage coils, using $i = j = 1$. Note that for calculation of absolute SNR in magnitude images, Eq. [9] constitutes an overestimate of the noise level (15), since the noise component orthogonal to the signal vector only minimally contributes to the apparent noise level.

Coil sensitivity profiles $\mathbf{\Sigma}$ for *g*-map calculation (Eq. [5]) were derived from the full *k*-space image data after additional processing steps to remove object contrast. Signal intensity contrast originating from the object structure was removed by dividing by the RSS combined image. Phase contrast was removed by subtracting a combined phase image, generated as follows. First, the phase in the center of the object was computed for each coil. Subsequently,

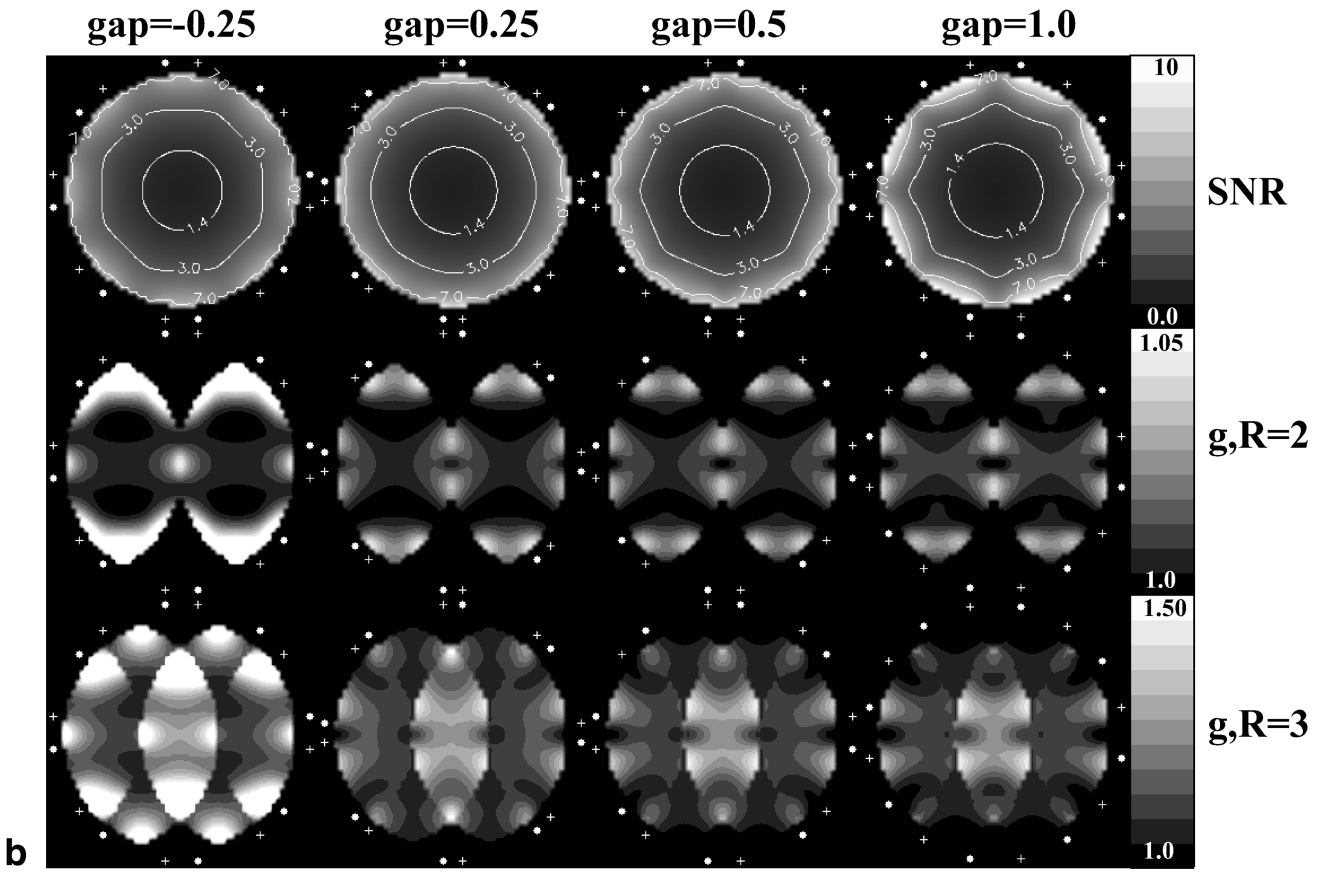

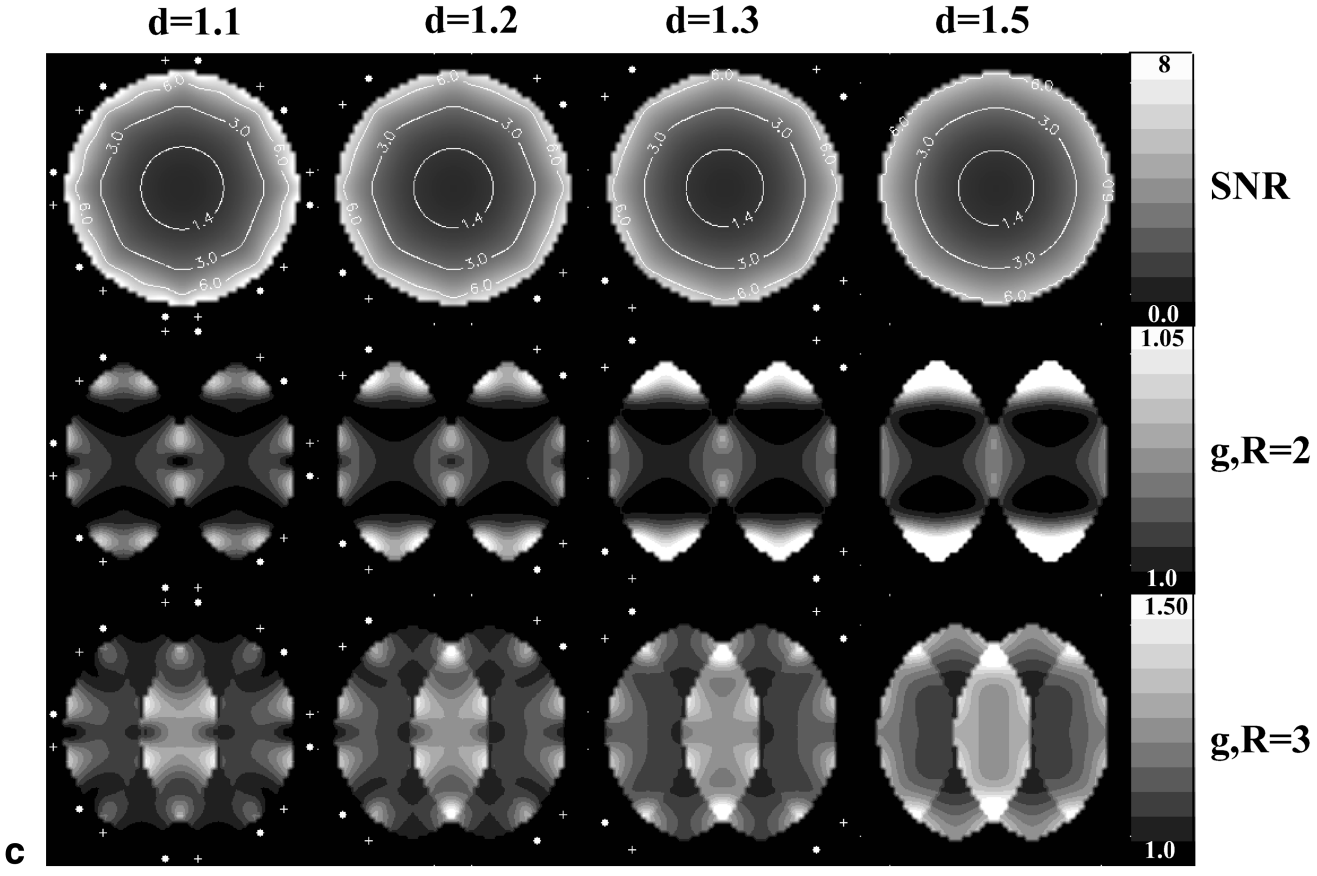

Figure 4. Continued.

Table 1
SNR and *g* as Function of Number of Coil Elements

# Elements	4	8	16	32
SNR in center	0.90	1.00	1.02	1.02
maximum SNR	6.18	10.37	27.58	95.81
average SNR	1.89	3.64	7.26	15.23
maximum *g*:				
rate-2	1.23	1.04	1.004	1.003
rate-3	6.60	1.64	1.10	1.09
rate-4	46.39	6.11	1.58	1.51
average *g*:				
rate-2	1.06	1.01	1.001	1.001
rate-3	1.99	1.14	1.03	1.02
rate-4	7.66	1.86	1.24	1.14

Table 2
SNR and *g* as Function of Gap

Gap	−0.25	0.25	0.50	1.00
SNR in center	0.98	1.00	1.00	0.99
maximum SNR	8.65	10.34	10.37	13.68
average SNR	3.12	3.51	3.64	3.84
maximum *g*:				
rate-2	1.16	1.06	1.04	1.03
rate-3	2.68	1.88	1.64	1.46
rate-4	8.80	7.03	6.11	5.13
average *g*:				
rate-2	1.03	1.01	1.01	1.01
rate-3	1.43	1.16	1.14	1.12
rate-4	2.74	2.00	1.86	1.74

Table 3
SNR and *g* as Function of Coil Diameter

Coil diameter	1.1	1.2	1.3	1.5
SNR in center	1.00	1.01	1.03	1.04
maximum SNR	10.37	7.90	6.86	5.98
average SNR	3.64	3.08	2.98	2.90
maximum *g*:				
rate-2	1.04	1.06	1.07	1.09
rate-3	1.64	1.71	1.92	1.98
rate-4	6.11	4.86	5.33	5.78
average *g*:				
rate-2	1.01	1.01	1.01	1.02
rate-3	1.14	1.16	1.18	1.21
rate-4	1.86	1.98	2.16	2.48

the difference in center phase with respect to the center phase in the first coil element was subtracted from the individual coil phase maps. Finally, a combined phase image was generated by taking the square root of squared magnitude weighted summation of individual coil phase maps. To all voxels more than five voxel dimensions away from the edge of the object, a 3 × 3 smoothing filter was applied. Polynomial fitting was performed to all pixels closer to the edge of the mask to obtain smoothing as well as coil sensitivity information in a 5-pixel wide ring surrounding of the object.

RESULTS

Simulations

Figure 4a–c and Tables 1–3 summarize the results of the coil field simulations. Figure 4a–c gives SNR and *g* at SENSE acceleration rates 2 and 3 under various conditions in a slice through the center of the object. Listed in Tables 1–3 are SNR in the center of the object, SNR closest to the center of the elements (maximum SNR), SNR averaged over the object (average SNR), and the maximum and average *g* within the object at SENSE rates 2, 3, and 4. SNR values are relative to the SNR calculated in the center of an 8-rung birdcage with $d_c = 1.1d_o$.

With increasing number of coil elements (Table 1, Fig. 4a), *n*, the maximum SNR increased, while *g* decreased. Both the maximum and average SNR rapidly increased with *n*, whereas SNR in the center only increased marginally. Both average and peak *g*-values decreased rapidly up until $n = 16$, after which the little change was observed.

Increasing the interelement gap (Table 2, Fig. 4b) from a 25% overlap ("gap" = −0.25) to a 100% separation ("gap" = 1) resulted in a substantial improvement in *g* as well as average and maximum SNR values. These improvements were mostly seen in the periphery (close to the conductors). The SNR in the center of the object showed a relatively weak dependence on "gap."

Increasing coil diameter d_c from 10–50% larger than the object diameter (Table 3, Fig. 4c) resulted in substantial deterioration of peak and average SNR. The same was true for peak and average *g*, except for the average *g* at acceleration rate 2, which was almost independent of d_c. On the other hand, central SNR improved slightly with increasing diameter.

The simulations also showed a dependency of *g*-maps on the coil orientation (rotation in axial plane) with respect to the SENSE-acceleration direction. In particular, the location and magnitude of g_{max} varied substantially with orientation. This dependency was most pronounced for coil arrays with fewer than eight elements and acceleration rates exceeding 2. The effect of orientation on the average *g*-value at the various acceleration rates was much smaller and almost insignificant. For the simulations with the various coil parameters described above, an element orientation was chosen that allowed building a coil that could easily be split in top and bottom half (to allow easy access and adaptation to various head sizes). This orientation did not always correspond to the orientation with the lowest g_{max} for all orientations (e.g., for an 8-element coil, elements at 0°, 45°, 90°, 135° etc., orientation would have resulted in 0%, 14%, and 12% lower values of g_{max} at rate 2, 3, and 4, respectively, compared to a 22.5° rotated version shown in Fig. 4 and Table 1).

Noise Resistance Measurements

Measurements on the test coils with varying diameter showed that coil noise and sample noise resistance R_c and R_s followed the expected behavior, i.e., a linear and third-power dependency on coil diameter of R_c and R_s, respectively. Furthermore, above coil diameters of 5 cm, sample noise became the dominant noise source. The fact that the elements in our 8-channel prototype were substantially larger than this (surface areas of around 75 cm^2), confirms the assumption that sample noise is indeed significantly larger than coil noise at 1.5 T.

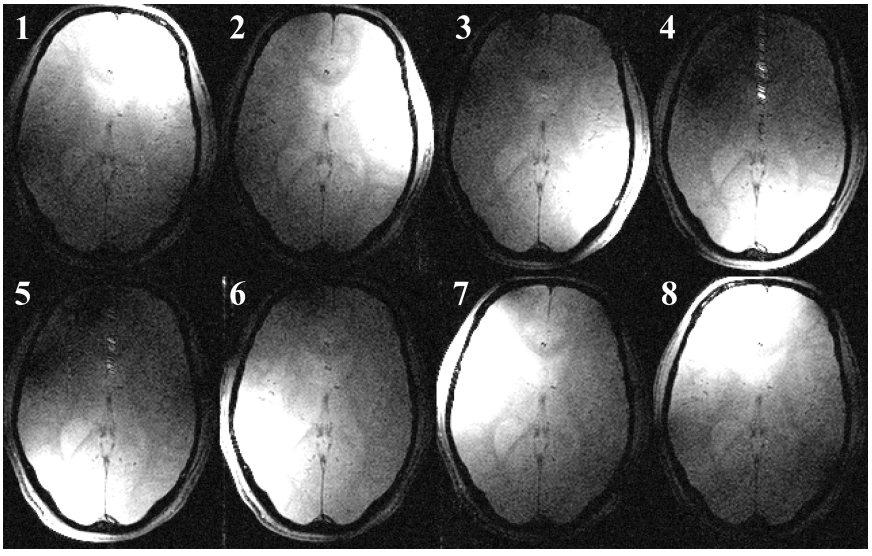

FIG. 5. Efficacy of preamplifier decoupling. The individual element images of an axial slice through the human brain, recorded with the prototype 8-channel brain coil, show minimal inductive coupling. Significant coupling would result in the "leakage" of one element's intensity pattern into one or more of the others'. Minor coupling effects (coupling estimated to be within 10%) from coil 8 into coils 3, 4, and 5 appear present, judging from the relatively dark area in elements 3, 4, and 5 in the sensitive area of coil 8.

MR Measurements

Figures 5 and 6 show results of MR measurements with the 8-channel brain coil on a normal volunteer. The individual coil images (Fig. 5) indicate an excellent orthogonality (small overlap) between the sensitivity profiles. In addition, there are only faint signs of inductive coupling between the elements, demonstrating the effectiveness of the preamplifier decoupling scheme. Estimated from these profiles the inductive coupling was less than 5% between most elements and between 5 and 10% from element 8 into elements 3, 4, and 5. These estimates were obtained by comparing the signal intensity in the proximity of coil *n* in the image from coil *m* with the signal intensity in the same location in the image obtained with coil *n*. The residual coupling was attributed to inaccurate phasing of the signal from channel 8 going into the preamplifier. Figure 6a,b demonstrates the excellent anatomical coverage achieved with the 8-channel coil. SNR levels exceeded those of the standard Siemens head coil throughout the brain (Fig. 6c,d). Averaged over the brain, SNR improved 2.7-fold, whereas some peripheral areas showed SNR gains exceeding a factor of 4. These measured gains were substantially lower than the values of 3.64 and 10.37 for simulated average and peak SNR gains, respectively. Central brain areas showed a 10% SNR improvement. These gains were similar (within 10%) when compared to the SNR of the General Electric head coil. SENSE *g*-values at rates 2 and 3 are given in Fig. 6e,f for an axial slice. Peak and average *g* were 1.15 and 1.06, respectively, at rate 2, and 2.01 and 1.38, respectively, at rate 3. Although these *g*-values indicate relatively little SENSE-related noise amplification, they are substantially higher than the peak/average *g* values of 1.04/1.01 at rate 2 and 1.64/1.14 at rate 3 found with the simulations.

DISCUSSION

Computer simulations showed that excellent SNR and SENSE performance can be achieved with arrays consisting of a large number of elements with a significant interelement gap and a close proximity to the head. This configuration leads to low values of *g*, as well as high average and peripheral SNR. With this configuration, central SNR is similar to configurations with 25% overlapping elements, or with coil diameters that are 50% larger than the object diameter, respectively.

SNR in the center of the object did not vary substantially with coil diameter, number of coil elements, or interelement gap. Some (around 10%) central SNR was lost with the 4-element coil. For all other geometries investigated, SNR in the center was within 10% of the SNR of the simulated birdcage coil. In absence of noise sources other than sample noise, this is to be expected, since in the center of the object signals from the different coil elements are added with equal weighting and with coherent phase, which is equivalent to the signal combining achieved through tuning in a birdcage coil.

The simulation results described above only included on-axis variation in the optimization space with dimensions including diameter, interelement gap, and number of elements. A limited number of off-axis variations were also simulated (e.g., simultaneous variation of both interelement gap and array diameter). This did not, however, lead to further design improvements.

For the construction of a prototype coil, there are a number of practical considerations, which were ignored in the simulations. These include the feasibility to eliminate noise sources not originating from the sample, as well as to eliminate inductive coupling between the elements. These issues were tackled using dedicated signal preamplifiers with high input impedance and low noise figure. This prototype showed both excellent SNR performance and low *g*-values over the entire brain, although not quite as good as suggested by the simulations. One possible source of this discrepancy is the difference between actual and simulated coil geometry. To facilitate the calculations in the computer simulations, the conductor layout was simplified. Although these simulations provided useful information, their accuracy was most likely inadequate to provide a quantitative standard for comparison with experi-

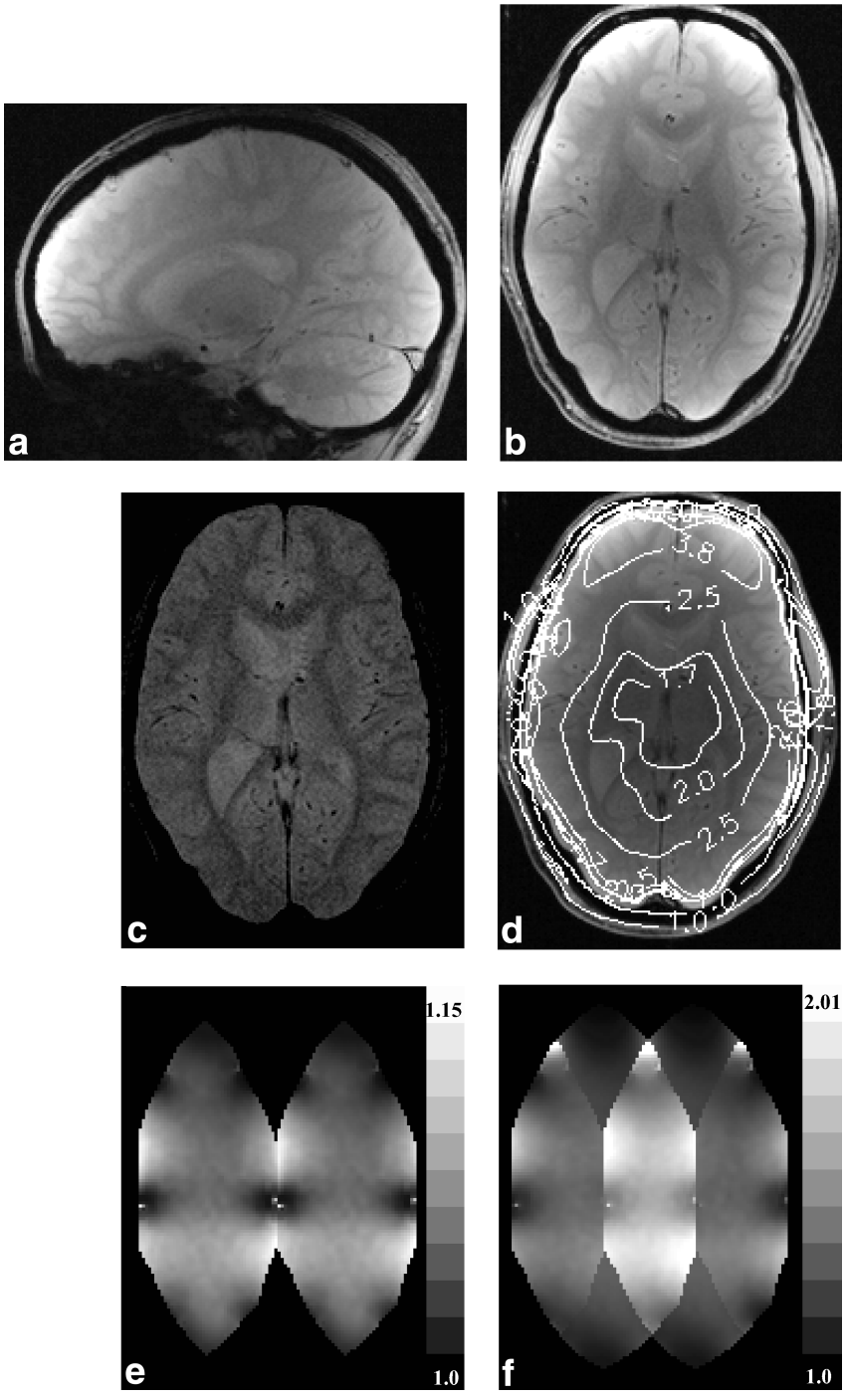

FIG. 6. Performance measurements on the prototype 8-channel brain array. Excellent coverage throughout the brain was achieved (**a,b**). Significant improvement in peripheral SNR was obtained as compared to the Siemens head coil (**c**). Images in **b** (brain array) and **c** (standard coil) have similar intensity scale. Relative improvements are indicated with the contours in **d**. SENSE performance is indicated in **e** and **f**, which show *g* at rates 2 and 3, respectively.

mental data. Another potential source of discrepancy is the oversimplification of the geometry and conductivity of the human head in the cylindrical model with uniform conductivity used in the simulations. Furthermore, the actual maximum SNR was derived from areas within the cortex, which is not as close to the coil elements as was simulated due to an additional separation imposed by scalp and skull.

The simulations suggest that potentially higher performance can be reached with more channels. A higher number of channels allows the use of smaller elements and facilitates a potential subdivision in the axial direction; for example, allowing for more than one row of elements with overlap in the axial direction (5). For the design presented above, the maximum number of elements is limited by inductive coupling and relative contribution of resistive

coil noise, both of which reduce SNR and increase with smaller coil size. Quality-factor measurements on individual square coils under loaded and unloaded conditions showed that, at 63.6 MHz, coil resistance becomes the dominant source of noise for coils with a surface area below 25 cm^2. This is generally undesirable, since it leads to a reduction of SNR in the center of the object. Therefore, the use of 20–30 coil elements appears optimal for brain imaging at 1.5 T. At higher fields, smaller coil sizes (i.e., more elements) are possible due to the increased contribution of sample loading to coil quality factor and overall noise resistance.

The simulations furthermore suggested that coil performance is affected substantially when only a few coil elements are used. When less than eight channels are available, as is the case with most clinical scanners today, peripheral SNR is reduced and both average and maximum *g*-values are increased. There are a number of ways to ameliorate this situation. First of all, reduction in *g* can be achieved by reducing the requirements on aliasing artifact rejection, e.g., through matrix regularization (16). Second, significant reductions in g_{max} can sometimes be achieved by slightly backing off (e.g., 10%) on the FOV reduction factor, i.e., in effect use fractional acceleration factors. Lastly, multiple elements could be combined into a single receiver channel. This allows the use of more coil elements than the available number of receiver channels, potentially leading to improved performance.

CONCLUSION

For brain MRI at 1.5 T, high SNR and SENSE performance can be achieved with a gapped array with a large number of elements in close proximity to the head and a substantial interelement gap. Measurements on a prototype 8-channel array show that effective inter-element decoupling can be achieved under practical conditions using preamplifiers with ultra-high input impedance. It is expected that a similar design can be used to build improved arrays by using more elements, especially at higher magnetic field strengths.

ACKNOWLEDGMENTS

The authors thank Alan Koretsky, Han Wen, and Scott Chesnick for helpful discussions.

REFERENCES

1. Hayes CE, Axel L. An efficient, highly homogeneous radiofrequency coil for whole-body NMR imaging at 1.5 T. J Magn Reson 1985;63:622–628.
2. Roemer PB, Edelstein WA, Hayes CE, Souza SP, Mueller OM. The NMR phased array. Magn Reson Med 1990;16:192–225.
3. Pruessmann KP, Weiger M, Scheidegger MB, Boesinger P. SENSE: sensitivity encoding for fast MRI. Magn Reson Med 1999;42:952–962.
4. Sodickson DK, Manning WJ. Simultaneous acquisition of spatial harmonics (SMASH): fast imaging with radiofrequency coil arrays. Magn Reson Med 1997;38:591–603.
5. Mansfield P, Pykett I. Biological and medical imaging by NMR. J Magn Reson 1978;29:355–373.
6. Bammer R, Keeling SL, Augustin M, Pruessmann KP, Wolf R, Stollberger R, Hartung HP, Fazekas F. Improved diffusion-weighted single-shot echo-planar imaging (EPI) in stroke using sensitivity encoding (SENSE). Magn Reson Med 2001;46:548–554.
7. de Zwart JA, Kellman P, van Gelderen P, Duyn JH. On the potential of sensitivity encoded EPI for BOLD functional brain imaging. In: Proc 9th Scientific Meeting, ISMRM, Glasgow, 2001. p 1217.
8. Porter JR, Wright SM, Reykowski A. 16-element phased array head coil. Magn Reson Med 1998;40:272–279.
9. Schäffter T, Börnert P, Leussler C, Carlsen IC, Leibfritz D. Fast ^1H spectroscopic imaging using a multi-element head-coil array. Magn Reson Med 1998;40:185–193.
10. Herlihy DJ, Larkman DJ, Fujita H, Burl M, Hajnal JV. A 4 channel head coil for SENSE imaging. In: Proc 8th Scientific Meeting, ISMRM, Denver, 2000. p 1394.
11. King SB, Duensing GR, Peterson D, Varosi S, Molyneaux DA. A comparison of 1, 4, and 8 channel phased array head coils at 1.5T. In: Proc 9th Scientific Meeting, ISMRM, Glasgow, 2001. p 1090.
12. Weiger M, Pruessmann KP, Leussler C, Röschmann P, Boesinger P. Specific coil design for SENSE: a six-element cardiac array. Magn Reson Med 2001;45:495–504.
13. Ledden PJ, Inati S. Four channel preamplifier decoupled phased array for brain imaging at 1.5T. In: Proc 9th Scientific Meeting, ISMRM, Glasgow, 2001. p 1117.
14. Wang J, Reykowski A, Dickas J. Calculation of the signal-to-noise ratio for simple surface coils and arrays of coils. IEEE Trans Biomed Eng 1995;42:908–917.
15. Hayes CE, Roemer PB. Noise correlations in data simultaneously acquired from multiple surface coil arrays. Magn Reson Med 1990;16:181–191.
16. Kellman P, McVeigh ER. SENSE coefficient calculation using adaptive regularization. In: Proc ISMRM Workshop on Minimum MR Data Acquisition Methods, Marco Island, FL, 2001. p 121–124.